A Baroclinic Instability that Couples Balanced Motions and Gravity Waves

Riwal Plougonven

National Center for Atmospheric Research, Boulder, Colorado

David J. Muraki

Simon Fraser University, Burnaby, British Columbia, Canada

Chris Snyder

National Center for Atmospheric Research, Boulder, Colorado

ABSTRACT

Normal modes of a linear vertical shear (Eady shear) are studied within the linearized primitive equations for a rotating stratified fluid above a rigid lower boundary. The authors' interest is in modes having an inertial critical layer present at some height within the flow. Below this layer, the solutions can be closely approximated by balanced edge waves obtained through an asymptotic expansion in Rossby number. Above, the solutions behave as gravity waves. Hence these modes are an example of a spatial coupling of balanced motions to gravity waves.

The amplitude of the gravity waves relative to the balanced part of the solutions is obtained analytically and numerically as a function of parameters. It is shown that the waves are exponentially small in Rossby number. Moreover, their amplitude depends in a nontrivial way on the meridional wavenumber. For modes having a radiating upper boundary condition, the meridional wavenumber for which the gravity wave amplitude is maximal occurs when the tilts of the balanced edge wave and gravity waves agree.

1. Introduction

Balanced motions and gravity waves are usually thought of in terms of superposition (e.g., Lorenz 1980), as in the weakly nonlinear analysis of small perturbations to a rotating fluid at rest (e.g., Blumen 1972; Dewar and Killworth 1995). In some contexts, however, balanced motions and gravity waves can be spatially coupled across a change in the environment such as a background shear; for example, in a two-layer baroclinic flow unstable modes can arise from the resonance of a Rossby wave with a gravity wave (Sakai 1989; Iga 1993). Although these waves have very different intrinsic time scales, the shear can make their Doppler-shifted frequencies coincide, and hence allow them to resonate. Similar unbalanced unstable modes, coupling balanced edge waves near the ground and gravity waves aloft, exist in rotating stratified fluid with a vertical shear, and will be the focus of this study.

Corresponding author address: Riwal Plougonven, Mathematical Institute, University of St. Andrews, St. Andrews KY16 9SS, United Kingdom.
E-mail: riwal.plougonven@polytechnique.org

Normal modes of a vertical linear shear have frequently been investigated, beginning with the classical baroclinic instability study by Eady (1949), which obtained the unstable modes under the quasigeostrophic (QG) approximation for a fluid bounded above and below by rigid surfaces. For a fluid unbounded above, the QG framework yields only neutral, traveling modes trapped near the lower boundary (Gill 1982, section 13.2); we will refer to such modes as quasigeostrophic edge waves. The unstable modes that are present when a rigid lid is added can then be interpreted as the resonance of two edge waves, one on the lower and one on the upper boundary (e.g., Hoskins et al. 1985).

Stone (1966) extended Eady's results both to meridionally varying modes and to the linearized primitive equations, hence including unbalanced effects. Stone (1970) and Tokioka (1970) independently identified unstable modes beyond the quasigeostrophic Eady cutoff. Tokioka showed that this unbalanced instability is associated with the singularity at an inertial critical level (Jones 1967). He also showed that the structure of these modes, though not their growth rate, depends strongly on the sign of the meridional wavenumbers.

Nakamura (1988) revisited these modes and the role of the inertial critical level (IL). He was the first to note

that the behavior of the solutions changed across the IL from a balanced edge wave to an inertia–gravity wave and to identify the mode as arising from the interaction of these two waves. Nakamura's analysis of the structure of the modes was extended to nonzero meridional wavenumber by Yamazaki and Peltier (2001b). One striking but unexplained feature of their solutions (see their Fig. 5) is that the gravity wave part of the modes appears to have a pronounced asymmetry in meridional wavenumber, with much greater amplitudes for horizontal wave vectors pointing toward the warm air in the direction of the shear.

The relevance of these unbalanced modes as instabilities is unclear for two reasons. First, in studies for meridionally uniform shear $U = \Lambda z$, the corresponding growth rates are found to be small for typical midlatitude Rossby numbers (Nakamura 1988; Yamazaki and Peltier 2001b). Molemaker et al. (2005) have revisited these modes and suggest that, despite their small growth rates, they may still have importance in providing a mechanism of energy transfer from the balanced manifold to unbalanced motions. Second, the manifestation of these modes in more realistic jets is uncertain. Snyder (1995) investigated numerically the linear stability of two-dimensional fronts $U(y, z)$ with uniform potential vorticity (PV). He identified synoptic-scale modes whose properties were well approximated by the quasigeostrophic equations, but found that unbalanced instabilities analogous to those of Stone (1970) and Tokioka (1970) either had growth rates too small to be detected by his numerical technique or were absent. Yamazaki and Peltier (2001a), on the other hand, considered jets with nonuniform PV and found a subsynoptic-scale instability with growth rates comparable to the synoptic-scale branch. It is not clear whether their subsynoptic-scale modes are counterparts of the unbalanced instabilities present with much smaller growth rates in meridionally uniform basic states or largely balanced instabilities associated with the interior PV gradients as in the classical study of Charney (1947).

Nevertheless, the unbalanced modes considered here are of interest for their structure: they serve as an illustration of how balanced motions and gravity waves are coupled spatially in a realistic stratified flow that is simple enough that the coupling can be analytically quantified. To our knowledge, the present study, together with that of Vanneste and Yavneh (2004), are the first in which the gravity waves are analytically quantified in terms of their Rossby number dependence.

The aim of this paper is to understand and quantify the spatial coupling of balanced motions and gravity waves in these simple baroclinic instabilities. The paper is organized as follows: the derivation of the equation for the vertical structure of the modes is presented in section 2. The role of the singularities in this equation are discussed in section 3, and it is shown that, to a first approximation, the modes consist of balanced motions below the IL and gravity waves above. In section 4, we show that it is possible to obtain analytically the amplitude of the gravity wave part of the modes as a function of the parameters. We illustrate this first in the case of neutral, meridionally uniform solutions. The more general case of modes with no restriction on the meridional wavenumber and with a radiating boundary condition aloft is then investigated in section 5. The dependence of the amplitude of the gravity waves on the meridional wavenumber is discussed in section 6. A discussion of the relevance of these results to the debate on the coupling of balanced motions and gravity waves is given in section 7, and our results are summarized in section 8.

2. The vertical structure equation

We use as our starting point the primitive equations for an f-plane geophysical fluid that is adiabatic, inviscid, and hydrostatic within the Boussinesq approximation (e.g., McWilliams and Gent 1980):

$$\frac{Du}{Dt} - fv + \phi_x = 0, \tag{1a}$$

$$\frac{Dv}{Dt} + fu + \phi_y = 0, \tag{1b}$$

$$\phi_z = \frac{g}{\theta_0}\,\theta, \tag{1c}$$

$$\frac{D\theta}{Dt} = 0, \tag{1d}$$

$$u_x + v_y + w_z = 0, \tag{1e}$$

where f is the Coriolis parameter, θ_0 is a reference potential temperature, g is the gravitational acceleration, ϕ is the geopotential height, and θ is the potential temperature; z is a modified pressure coordinate (Hoskins and Bretherton 1972), but we will refer to it simply as height.

The primitive equations are linearized around a basic state of constant vertical shear and constant stratification. The basic-state zonal wind and potential temperature are given by

$$U(z) = \Lambda z, \quad \Theta_S(y) = -\frac{f\theta_0\Lambda}{g}\,y, \tag{2}$$

where the shear Λ is constant.

Using horizontal and vertical length scales L and H, respectively, and a velocity scale ΛH, the nondimensional equations are

$$\mathcal{R}Du + \mathcal{R}^2 \bar{\Lambda} w - v + \phi_x = 0, \tag{3a}$$

$$\mathcal{R}Dv + u + \phi_y = 0, \tag{3b}$$

$$D\theta - \bar{\Lambda} v + \mathcal{B} w = 0, \tag{3c}$$

$$\phi_z = 0, \tag{3d}$$

$$u_x + v_y + \mathcal{R} w_z = 0, \tag{3e}$$

where $D = \partial_t + \bar{\Lambda} z\, \partial_x$ includes advection by the shear, $\mathcal{R}$ is the Rossby number, and $\mathcal{B}$ is the Burger number, which we can assume without loss of generality to be unity:

$$\mathcal{R} = \frac{\Lambda H}{fL}, \quad \mathcal{B} = \left(\frac{NH}{fL}\right)^2 = 1. \tag{4}$$

The parameter $\bar{\Lambda}$ is 1; we have left it in the equations to keep track of the role of the shear.

The above equations can be combined to give equations for the divergence of the horizontal wind and for the vertical component of the vorticity. These can in turn be combined with the other equations to yield one unique equation for w (Eady 1949; Jones 1967; Inverarity and Shutts 2000):

$$D(\mathcal{R}^2 D^2 + 1)w_{zz} - 2\bar{\Lambda}(\partial_x - \mathcal{R}D\partial_y)w_z$$
$$+ (D\Delta_H - \mathcal{R}2\bar{\Lambda}^2\partial_{xy})w = 0. \tag{5}$$

We consider propagating wave solutions of the form

$$w(x, y, z, t) = \text{Re}\{W(z)e^{i[k(x - \bar{\Lambda}\sigma t) + ly]}\}, \tag{6}$$

where the real part of σ can be considered a height such that $\bar{\Lambda}\text{Re}(\sigma)$ is the phase speed of the wave in the x direction. The growth rate (or decay rate) of the solution is given by $k\bar{\Lambda}\text{Im}(\sigma)$. For all the figures below, we will assume without loss of generality k equal to 1.

Inserting (6) into (5), the problem is reduced to a second-order ordinary differential equation (ODE) for the vertical structure of the vertical velocity

$$(z - \sigma)[1 - \mathcal{R}^2 k^2 \bar{\Lambda}^2(z - \sigma)^2]W'' - 2[1 - il\mathcal{R}\bar{\Lambda}(z - \sigma)]W'$$
$$- [(z - \sigma)\lambda^2 + \mathcal{R}2il\bar{\Lambda}]W = 0, \tag{7}$$

where $\lambda = \sqrt{k^2 + l^2}$, and the primes indicate derivatives of $W(z)$. We wish to determine both the eigenfunction $W(z)$ for $z \geq 0$ and the eigenvalue σ, with a lower boundary condition

$$W(0) = 0 \tag{8}$$

and an upper boundary condition to be discussed in section 5.

3. Two regions of vertical structure

An important feature of the vertical structure Eq. (7) is that the coefficient of the second derivative term, a cubic polynomial in z, can be zero. The roots of the leading coefficient in a linear differential equation are called the singular points (Braun 1993) and identify possible locations for singularity in the solutions. For most solutions of interest, the eigenvalue will turn out to be complex, so these singular points will not directly affect the solution along real values of z. Nonetheless, one of these singular points is associated with the iner-

tia critical level (IL) where the solutions make a transition from balanced to gravity wavelike structure.

Below we present a brief analysis of the singular points (section 3a) from which the construction of the nonsingular neutral mode of (7) follows. We then use approximate solutions to show that the solutions behave as balanced edge waves near the surface (section 3b) and gravity waves aloft (section 3c).

a. Analysis of the singular points

Three singular points of the vertical structure Eq. (7) are obtained from a factorization of the leading coefficient

$$z_{\text{CL}} = \sigma, z_{\text{IL}}^{\pm} = \pm \frac{1}{\mathcal{R}k\bar{\Lambda}} + \sigma. \tag{9}$$

For a real value of σ, these singular points are also real valued and identify important spatial transitions in the vertical structure of the solution $W(z)$ on $0 \leq z < +\infty$. The point at z_{CL} corresponds to a critical level (CL), a height at which the shear velocity exactly matches the phase velocity of the wave. The points $z_{\text{IL}}^{\pm}$ correspond to two ILs, heights at which the Lagrangian time scale based on the horizontal wavelength of the wave and phase velocity relative to the background shear is equal to the inertial period. When σ has a nonzero imaginary part, these singular features are no longer realized on the real z axis. Nevertheless, the singularities will still be present in the complex plane and, if $\text{Im}(\sigma)$ is not too large, will retain their significance for solutions on the real line near z_{CL} and $z_{\text{IL}}^{\pm}$.

The method of Frobenius (Braun 1993) provides a construction of solutions near a singular point z_s in the form of a series

$$W(z) = (z - z_s)^{\gamma}[1 + c_1(z - z_s) + c_2(z - z_s)^2 + \cdots]. \tag{10}$$

For a second-order ODE of the form

$$p(z)W'' + q(z)W' + r(z) = 0, \tag{11}$$

the two independent solutions at each z_s correspond to values of γ given by the roots of the quadratic indicial polynomial

$$\gamma(\gamma - 1) + \left[\lim_{z \to z_s} \frac{(z - z_s)q(z)}{p(z)}\right]\gamma$$
$$+ \left[\lim_{z \to z_s} \frac{(z - z_s)^2 r(z)}{p(z)}\right] = 0. \tag{12}$$

Generally, each of the two indicial roots generates a distinct series (10), and the pair form the two linearly

independent solutions expected for a second-order ODE.

For the vertical structure Eq. (7), the singular point $z_{CL} = \sigma$ has indicial roots $\gamma = 0$ and $\gamma = 3$. Thus, all solutions $W(z)$, including the first and second derivatives, are nonsingular at z_{CL}. Although generically it would be expected that the third and higher derivatives are singular, this turns out not to be the case and the singular point is completely removable from the vertical structure equation (see appendix A). Nonetheless, the CL still introduces a problem for many numerical ODE integrators since the $\gamma = 3$ solution is highly degenerate, with $W(z_{CL}) = W'(z_{CL}) = W''(z_{CL}) = 0$. Appendix A describes the numerical technique used in this case.

The Frobenius analysis for the remaining singular points $z_{IL}^{\pm}$ gives indicial roots of $\gamma = 0$ and $\gamma = \pm il/k$. For $l \neq 0$, the complex power in the solution (10) represents a logarithmic singularity at the IL. The situation is no different in the $l = 0$ case since the double root $\gamma = 0$ represents an exceptional case in Frobenius theory and also generates one solution with a logarithmic singularity. In both cases, the $\gamma = 0$ solution represents the unique (up to an amplitude scaling) nonsingular solution. However, only in the $l = 0$ case does the $W(0) = 0$ surface boundary condition yield a real eigenvalue σ. This solution has been computed and is shown in Fig. 1 for $l = 0$ and $\mathcal{R} = 0.5$, normalized so that $W(z_{CL}) = 1$. The numerically obtained eigenvalue is $\sigma \approx 0.9392$. This neutral, propagating solution is the counterpart within the linearized primitive equations to the quasigeostrophic edge wave (Gill 1982, section 13.2). The primitive equation solution shown in Fig. 1 oscillates aloft, unlike the quasigeostrophic edge wave that decays exponentially with height above the maximum of W. While Fig. 1 gives no visible indication that the IL is a singular point, it in fact separates a region near the surface, in which the solution may be approximated by a balanced edge wave, and the region aloft, in which the
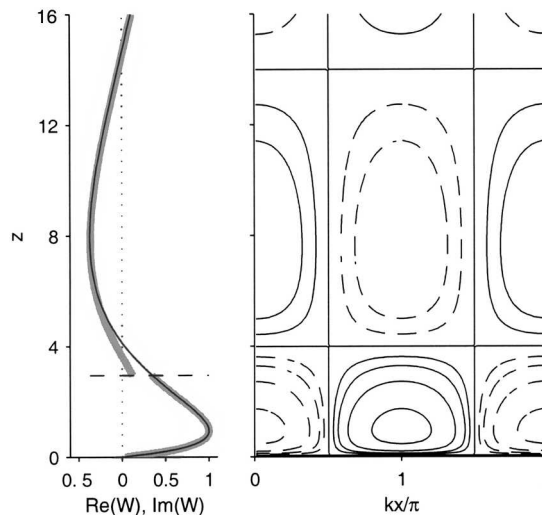

FIG. 1. Neutral solution for $\mathcal{R} = 0.5$, $l = 0$. In the left panel are superposed the numerically obtained solution (plain black line), and the asymptotic solutions [(13) and (15a), thick gray line] above and below the IL, indicated by the horizontal dashed line. Contours are 0, 0.1, 0.2, 0.4, 0.8, and their negative counterparts.

solution is close to an inertia–gravity wave in shear. We derive these approximations to the solution in the following subsections.

b. Balanced edge wave part

For small $\mathcal{R}$, we solve (7) asymptotically. This approach is valid near the ground, where the terms multiplied by $\mathcal{R}$ are indeed small. The approximation breaks down at heights where $(z - \sigma)$ becomes of the order $1/\mathcal{R}$, that is, near and above the IL [cf. Eq. (9)]. Hence, this approximate solution ignores the existence of the IL.

The solutions have been obtained up to second order in $\mathcal{R}$:

$$W_b(z) = e^{-\lambda(z - \sigma_b)}\left([\lambda(z - \sigma_b) + 1] + \mathcal{R}i\frac{l\bar{\Lambda}}{\lambda}[1 - \lambda^2(z - \sigma_b)^2] + \mathcal{R}^2\frac{\bar{\Lambda}^2}{2}\left\{\frac{\lambda k^2}{6}[(z - \sigma_b)^3 - 2\lambda(z - \sigma_b)^4]\ldots\right.\right.$$
$$\left.\left. + \frac{l^2}{\lambda}[2(z - \sigma_b) + 2\lambda(z - \sigma_b)^2 - \lambda^2(z - \sigma_b)^3]\right\} + O(\mathcal{R}^3)\right),$$

$$(13)$$

where subscript b indicates that this is the balanced solution. The phase speed σ_b is obtained by imposing the boundary condition (8) to expression (13):

$$\sigma_b = \frac{1}{\lambda} - \mathcal{R}^2\frac{\bar{\Lambda}^2}{4\lambda}\left(1 - \frac{3l^2}{\lambda^2}\right) + O(\mathcal{R}^3). \qquad (14)$$

Note that the correction to σ_b is real so that the mode is neutral.

The leading order parts of (13) and (14) are the quasigeostrophic edge waves (Gill 1982, section 13.2). These waves propagate in the direction of the shear and are trapped near the surface. To leading order, the maximum of the vertical velocity occurs at the criti-
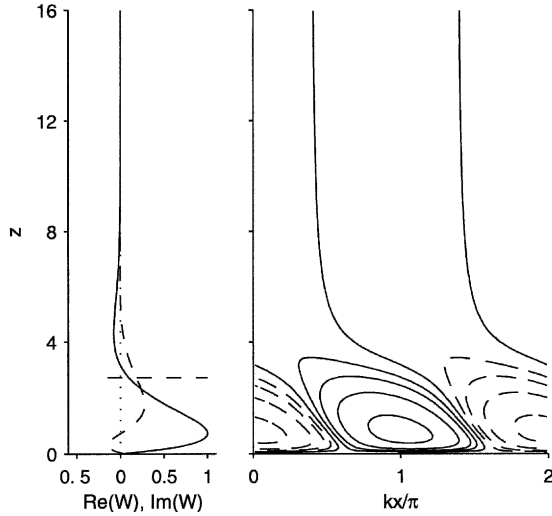
FIG. 2. The balanced edge wave solutions for $\mathcal{R} = 0.5$ and $l = -1$, obtained asymptotically in $\mathcal{R}$ up to second order from (13). The format is as in Fig. 1 with the addition of $\text{Im}(W_b)$ (dashed) in the left panel.

cal level, and these solutions are normalized so that $W_b(\sigma_b) = 1$.

For $l = 0$ the solutions are real. For $l = 0$ and $\mathcal{R} = 0.5$ the asymptotic solution (13) is shown in Fig. 1 below the IL as a thick gray line. Thus, the full solution is well approximated as a balanced edge wave below the IL. At $\mathcal{R} = 0.5$, the phase speed of the solution, $\sigma \approx 0.9392$, is also well approximated by $\sigma_b = 0.9375$.

For $l \neq 0$, the $O(\mathcal{R})$ correction introduces an imaginary part to the solution. The solution then tilts in the (x, z) plane (McIntyre 1965), as shown in Fig. 2, and in the (y, z) plane. Since the $O(\mathcal{R})$ correction is proportional to l, the sense of the tilt in the (x, z) plane depends on the sign of l, while that in the (y, z) plane does not. These tilts will be discussed further in section 6.

c. Inertia–gravity wave part

For large $z \gg z_{CL}$, we look for solutions expressed as power series; this is akin to applying the method of Frobenius at a point at infinity (Braun 1993). Keeping only the highest powers of $(z - \sigma)$ in (7), we find that leading order solutions in the far field have the form

$$W(z) \sim \alpha_1(z - \sigma)^P + \alpha_2(z - \sigma)^{P*}, \quad (15a)$$

$$\text{with} \quad P = \frac{1}{2} + i\mu, \mu = \sqrt{\text{Ri}\left(1 + \frac{l^2}{k^2}\right) - \frac{1}{4}}, \quad (15b)$$

where α_i are the waves' amplitudes and $\text{Ri} = (\mathcal{R}\bar{\Lambda})^{-2}$ is a Richardson number. The powers P and $P*$ have also been obtained from a quadratic indicial equation. For $\bar{\Lambda} > 0$, the first term in the solution corresponds to a gravity wave propagating upward (Booker and Bretherton 1967), that is, tilting against the shear as in

Fig. 3. The second term having the conjugate power, $P*$, is a downward propagating gravity wave. Higher-order corrections to these waves can be obtained perturbatively.

The neutral eigenmode shown in Fig. 1 is real and so should be compared against (15a) with $\alpha_2 = \alpha_1^*$, which yields a standing wave above the IL. This asymptotic solution, for $l = 0$, $\mathcal{R} = 0.5$ and with σ given by the edge wave approximation (14), is plotted as a gray line for $z > z_{\text{IL}}$ in the left panel of Fig. 1. The agreement shows that the solutions are well described above the IL as a superposition of upward and downward propagating gravity waves. An important conclusion from this example is that a neutral solution to (7) can only exist (for finite $\mathcal{R}$) when coupled to downward propagating waves. Neutral modes result if a rigid lid is placed at one of the discrete heights where $W(z) = 0$. Otherwise, in an unbounded fluid, these neutral modes require a wave source at infinity. In an unbounded fluid, the more physically meaningful wave solutions are those with only outgoing waves ($\alpha_2 = 0$) aloft, and such solutions will be discussed in section 5. In the next section, we show how Eq. (7) can be solved analytically; this allows us to understand the neutral solutions and more generally in all solutions to quantify the amplitude of the gravity waves relative to those of the balanced motions.

4. The connection problem

In the previous section we showed that the modes comprise a balanced edge wave below the IL and a gravity wave above, but their relative amplitudes could not be determined. This issue of asymptotic matching across the IL is an example of a connection problem (Bender and Orszag 1978). Such connection problems
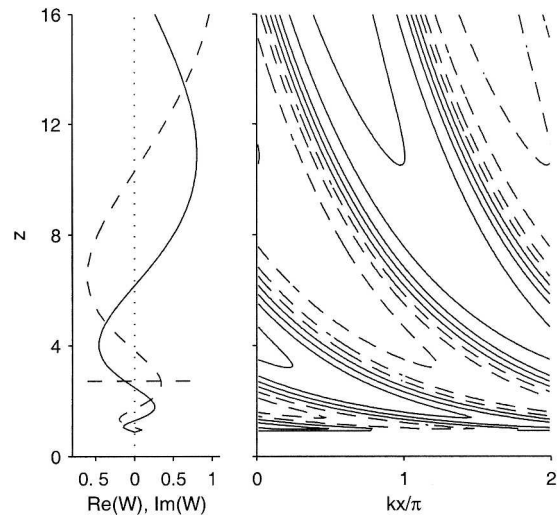

FIG. 3. As in Fig. 2 but for the far-field, upward propagating gravity wave solutions obtained for large $z - \sigma_b$ (15a).

are usually resolved by the use of special functions whose asymptotics are known. Here, the connection is resolved using the work of Yamanaka and Tanaka (1984) who found changes of variables that transform Eq. (7) into the canonical differential equation for the hypergeometric function (Abramowitz and Stegun 1964, hereafter AS, section 15.5.1). Recently, this transformation has been used in studies of steady flow over topography (Shen and Lin 1999; Wurtele et al. 2000; Shutts 2001, 2003). Shutts (2001) also notes that unstable modes of a linear shear flow can be obtained using that transformation. Here, this transformation allows us to obtain analytically, to an excellent approximation (see appendix B), the amplitude of the gravity waves as a function of the parameters.

The first change of variable incorporates the eigenvalue σ into the independent variable:

$$\xi = \mathcal{R}\bar{\Lambda}k(z - \sigma). \qquad (16)$$

A new function Y is then defined by

$$W(\xi) = (1 + \xi)^{-il/k}Y(\xi). \qquad (17)$$

Finally, the independent variable is changed to

$$\eta = \xi^2. \qquad (18)$$

This transforms (7) into the differential equation for hypergeometric functions (cf. AS, section 15.5.1):

$$\eta(1 - \eta)Y'' + [c - (a + b + 1)\eta]Y' - abY = 0, \qquad (19a)$$

with

$$a = -\frac{P^*}{2} - i\frac{l}{2k}, b = -\frac{P}{2} - i\frac{l}{2k}, c = -\frac{1}{2}, \qquad (19b)$$

and P given by (15b). Solutions to this equation, along with many asymptotic properties, are well established.

In the rest of this section, we illustrate the method to obtain the amplitude of the gravity wave part of the solution for the special case of the neutral mode (σ real), with $l = 0$, as presented in Fig. 1. As determined by the Frobenius analysis, there is only one solution that remains finite at the IL. From AS (section 15.5.5), this solution is denoted by

$$Y_n(\eta) = AF(a, a^*, 1, 1 - \eta), \qquad (20)$$

where F is the hypergeometric function and the subscript n refers to neutral. Hence, in the case of neutral solutions with $l = 0$, the classical hypergeometric function provides an exact analytical solution.

Now, to normalize (20) and obtain its far-field as-ymptotics, we use standard linear transformations and the fact that $F(a, b, c, 0) = 1$, for all a, b, and c. An equivalent expression of (20) is obtained (AS, section 15.3.6) involving a hypergeometric function with η as its fourth argument. This allows the mode to be normalized so that its value is unity at the critical level, $\eta = 0$. Another expression equivalent to (20) can be obtained (AS, section 15.3.8) such that the hypergeometric functions involved have $1/\eta$ as their fourth argument. These functions then tend to 1 as $\eta \to +\infty$. After working back through the changes of variables, this process determines the amplitude of $\alpha_1 = \alpha_2^*$ in (15a) to be

$$\alpha_n = (\mathcal{R}\bar{\Lambda}k)^P \frac{\Gamma(i\mu)\Gamma(5/4 - i/2\mu)}{\Gamma(3/2)\Gamma(-1/4 + i/2\mu)}, \qquad (21)$$

where $\Gamma(z)$ denotes the Gamma function and the subscript n refers to neutral. This amplitude was used to plot the gray line for the neutral wave of Fig. 1. For small Rossby number, the amplitude expression (21) can be further approximated using the fact that the parameter $\mu = O(\mathcal{R}^{-1})$. This gives

$$|\alpha_n(\mathcal{R}, k, \bar{\Lambda})| \sim \frac{2\sqrt{2k}}{\sqrt{\bar{\Lambda}}} \frac{1}{\sqrt{\mathcal{R}}} e^{-\pi/2\mathcal{R}\bar{\Lambda}} \quad \text{for} \quad \mathcal{R} \to 0, \qquad (22)$$

so that these gravity waves are seen to be of exponentially small amplitude in Rossby number. Note that this result bears some similarity with the amplitude of the edge wave at the IL where an exponential dependence on $\mathcal{R}$ is also obtained from ze^{-z} evaluated at $z_{\text{IL}}^+ = O(1/\mathcal{R})$. The relevance of this analytical result to previous studies on the coupling of gravity waves and balance is discussed in section 7.

5. Radiating modes

In the previous sections, we focused on neutral, meridionally uniform modes in order to discuss the singular points of the equation (section 3a) and to illustrate how α can be obtained analytically (section 4). For neutral modes, the requirement that the solutions remain bounded at the IL determines the form of the solution at large heights to be a mix of upward and downward propagating waves and, thus, leaves no freedom for specifying conditions at infinity. We now turn to the case with a radiating boundary condition aloft. The solutions then include unstable modes, on which we will focus, and decaying modes. They are automatically bounded near the IL since Eq. (7) no longer has singular points for real values of z.

The upper boundary condition used to identify upward propagating waves is deduced from (15a) and is given, along with the numerical technique used to obtain the modes, in appendix A. In his study of the
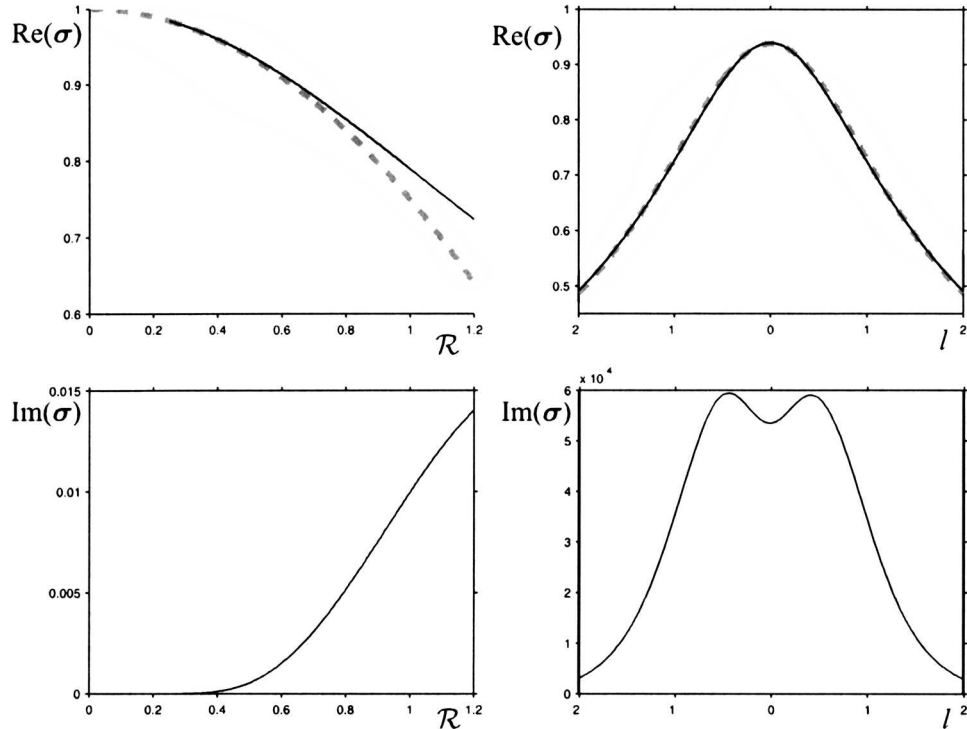
FIG. 4. Phase speed of the solutions Re(σ) and growth rates Im(σ) of the numerically obtained solutions (plain lines) as a function of $\mathcal{R}$ for $l = 0$ and as a function of l for $\mathcal{R} = 0.5$. Also plotted in the upper panels is the phase speed of the balanced edge wave σ_b (dashed line), obtained from the asymptotic solutions for small Rossby number.

weakly unstable unbalanced modes in a fluid with a rigid lid, Nakamura (1988) speculated that the rigid lid itself was not necessary for instability. We confirm this by showing that unstable modes exist when the lid is replaced by an outgoing radiating condition.

The numerically obtained values for the phase speed, Re(σ) have been compared with σ_b (14). As can be seen from Fig. 4, they compare well up to moderate Rossby numbers $\mathcal{R} \sim 0.6$ and over a wide range of l. This further confirms that the flow near the ground is well described by the balanced approximation (13), and indicates that the phase speed of the mode is controlled by the balanced component near the ground.

Solutions for different values of l are shown in Fig. 5. Here again, the IL retains its significance: as can be seen from the asymptotic solutions superposed as gray lines, the solutions make a transition at the IL from a balanced edge wave below to a gravity wave above. The gravity waves are strikingly larger for negative l than for positive l, as noted by Yamazaki and Peltier (2001b) in their case with an upper lid. A possible explanation for this asymmetry will be given in section 6.

The growth rates of these solutions are small, and hence the coefficient of the highest order term in (7) becomes very small in the vicinity of the IL. This can lead to very intense gradients near the IL (see the solution for $l = +1$ in Fig. 5). However, this is not nec-

essarily the case, and there are considerable intervals of l for which the solutions transition smoothly from the balanced edge wave below the IL to the gravity wave above, (see the solution for $l = -1$ in Fig. 5). These are also the solutions where the gravity waves are the most intense.

As the Rossby number is increased, the amplitude of the gravity wave part of the solution increases, the growth rates increase, and correspondingly the transition at the IL becomes smoother (see Fig. 6).

Now, as in the case of the neutral solutions with $l = 0$, it is possible to obtain the amplitude of the gravity wave part of the solution analytically. For complex σ, two linearly independent and bounded solutions exist. They are combined to obtain a solution verifying the radiating boundary condition aloft. Normalization of the solution then yields an analytical expression for α_u, the amplitude of the gravity waves, where the subscript u refers to unstable. Contrarily to the case of the neutral modes, the derivation of α_u [see appendix B and expression (37)] involves a slight approximation. Nevertheless, α_u compares extremely well with the numerical results, as can be seen from Figs. 7 and 8.

For small $\mathcal{R}$, an asymptotic expression is obtained for $|\alpha_u|$. It retains in a compact formula the essential dependences of the amplitude of the gravity waves on the parameters
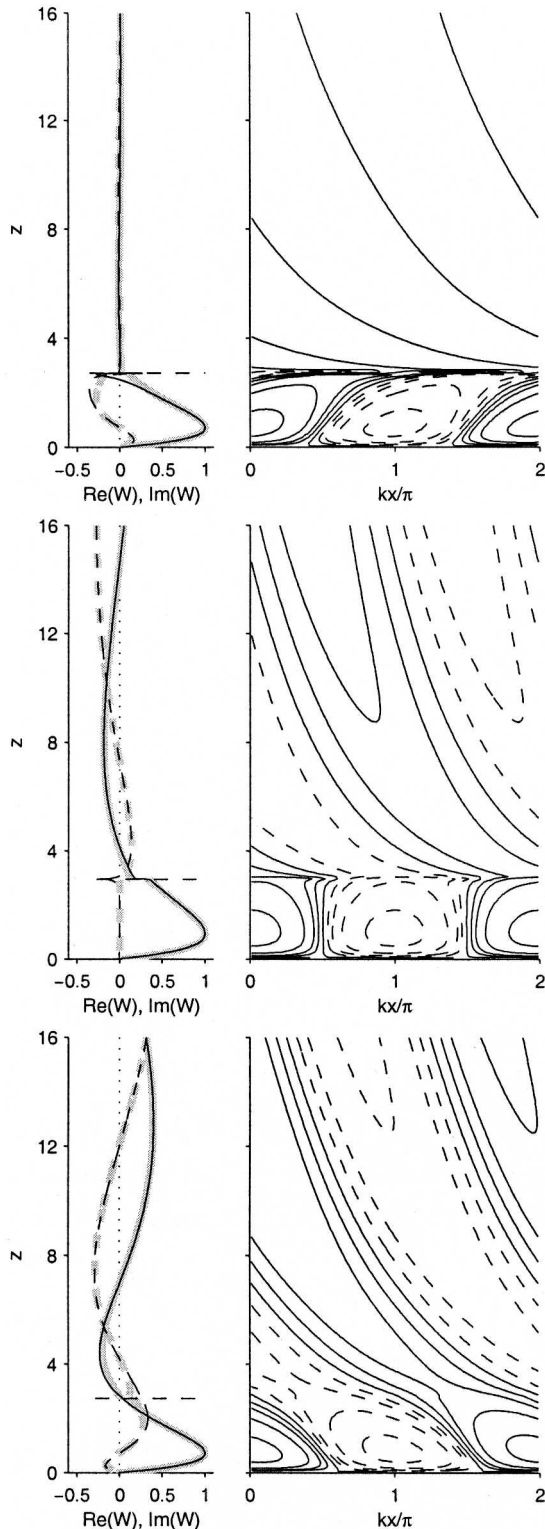
FIG. 5. As in Fig. 1 but for unstable modes at $\mathcal{R} = 0.5$ with a radiating upper boundary condition and (top) $l = 1$, (middle) $l = 0$, or (bottom) $l = -1$.
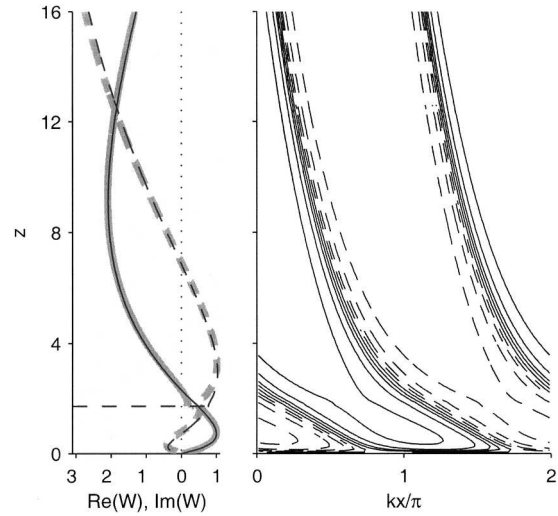

FIG. 6. As in Fig. 5 but for $\mathcal{R} = 1$, $l = -1$: the IL is lower, the amplitude of the waves is larger, and their vertical wavelengths are longer.

$$|\alpha_u(\mathcal{R}, k, l, \bar{\Lambda})| \sim \sqrt{k/\bar{\Lambda}} e^{-\pi l/2k} \frac{1}{\sqrt{\mathcal{R}}}$$

$$\exp\left[-\frac{\pi}{2\mathcal{R}\bar{\Lambda}} \sqrt{1 + l^2/k^2} \right],$$

$$\text{for} \quad \mathcal{R} \to 0. \qquad (23)$$

Here again the amplitude of the gravity waves is exponentially small in Rossby number. However, the dependence on the meridional wavenumber is also important: note in particular the factor $e^{-\pi l/2k}$, which introduces an asymmetry in the meridional wavenumber l. An interpretation of this is given in the following section.

6. Meridional asymmetry

An asymmetrical dependence on l of solutions near the IL has already been noted by Tokioka (1970), Yamanaka and Tanaka (1984), Yamazaki and Peltier (2001b), and Shutts (2001). Shutts suggested that this asymmetry is related to the horizontal thermal gradient. Our study of the structure of the solutions has suggested that the amplitude of the gravity waves is related to how smoothly they match with the balanced part of the solution at the IL, as is discussed below. However, the physical reasons for this asymmetry are not yet understood.

From plots of $|\alpha_u|$ as a function of l (Fig. 8), it is seen that for each Rossby number there is a preferred meridional wavenumber $l_0(\mathcal{R})$ for which the amplitude of the gravity waves is maximized. Based on the simple asymptotic solutions obtained in section 3, we suggest that the preferred meridional wavenumber l_0 is that which allows the structures of the balanced edge wave
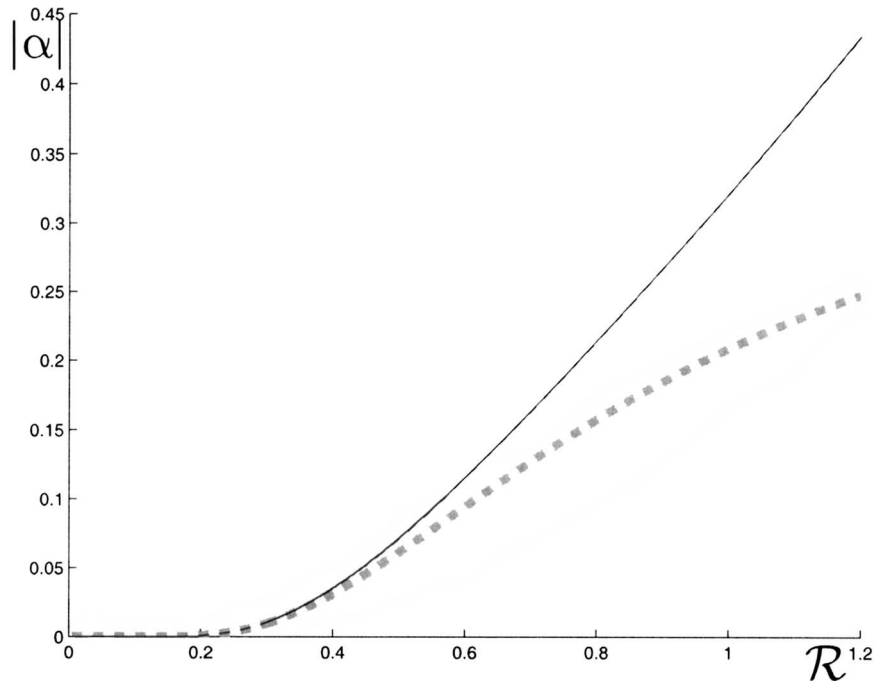
FIG. 7. Numerically obtained amplitude of the gravity waves $|\alpha_u|$ (plain line), with $l = 0$. Superposed are the analytically obtained value (B8) (dashed line) and its asymptotic expression for small Rossby number (23) (thick gray dashed line).

and of the gravity waves to match most smoothly at the IL. We review below, successively for the gravity wave and for the balanced edge wave, the dynamical constraints on the tilts of the phase lines in both the xz and in the yz plane.

The gravity wave part of the solution necessarily corresponds to waves propagating energy upward; hence their phase lines must tilt against the flow in the xz plane (Figs. 3 and 5). This requires that the phase lines in the yz plane tilt northward (in the same sense as the isentropes) for $l < 0$ and southward for $l > 0$, as shown in Fig. 9.

For the balanced edge wave part of the solutions, as was noted in section 3b, the $O(\mathcal{R})$ corrections in Eq. (13) introduce a tilt of the solutions; this tilt in the yz plane is always along the isentropes, that is, northward (see Fig. 9). Thus, in the xz plane, the phase lines of the balanced edge wave tilt westward for $l < 0$ and eastward for $l > 0$, as shown in Fig. 5 (see also Fig. 12 of Tokioka 1970). As a consequence, as can be seen from vertical cross sections in both the xz and yz planes (Figs. 5 and 9), the transition from the structure of the balanced edge wave to that of the gravity waves will be smoother for $l < 0$.

The illustrations are strongly suggestive of this.[1] To

check the relevance of this argument more quantitatively, we have proceeded to the following calculation: the tilts in the xz and yz planes at or near the IL for the gravity wave and the balanced edge wave part of the modes were calculated from the asymptotic solutions (13) and (15a). For each value of $\mathcal{R}$, there is a preferred meridional wavenumber l_{0x} that minimizes the differences in the tilts in the xz plane; there is another value l_{0y} that minimizes the differences in the tilts in the yz plane. If the above argument is correct, we should expect that the value of l that maximizes the amplitude of the gravity waves is a compromise between these two values, or at least has a similar evolution with $\mathcal{R}$. Figure 10 shows that this is indeed the case. This calculation cannot, however, be made very precise since the asymptotic expression for the balanced edge wave part of the solution fails at the IL (cf. section 3b). As a consequence, the calculation of the preferred tilts in the xz and yz plane from this asymptotic expression is problematic, and we calculate the tilts not at the IL but slightly below. Thus there is a measure of arbitrariness in the height chosen.

7. Discussion

Although these unbalanced baroclinic modes have been known to exist for some time, their relevance regarding the coupling of balanced motions and gravity waves and the question of the slow manifold has not

---

[1] These observations do not apply when a rigid lid is present as in Yamazaki and Peltier (2001b, their Fig. 5), although the same asymmetry in l is found.
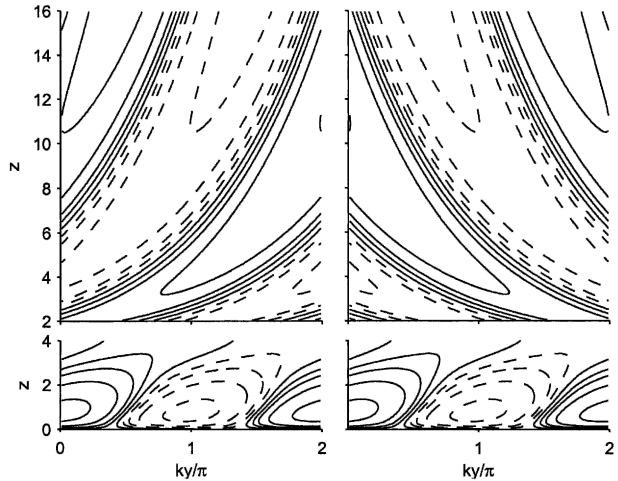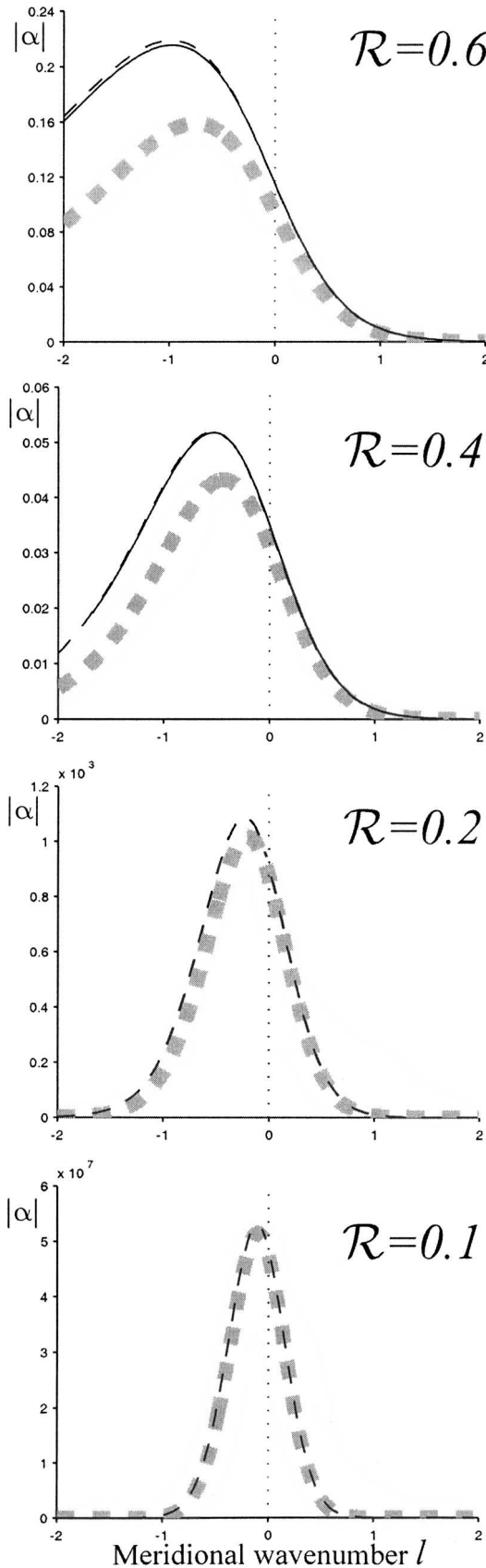
FIG. 9. Contour plots in the (yz) plane (top) of the gravity wave solutions (15a), and (bottom) of the balanced edge wave solution (13), for $\mathcal{R} = 0.5$, and with (left) $l = -1$ and (right) $l = 1$. The IL is located at $z \approx 2.73$.

previously been discussed.[2] Because the time scales for balanced motions and gravity waves are well separated for synoptic motions, it has been suggested that the two types of motions decouple, leading to the notion of the slow manifold (Leith 1980; Lorenz 1980). Evidence that this decoupling could not be complete first came from investigations of highly truncated, reduced models (e.g., Vautard and Legras 1986; Lorenz and Krishnamurty 1987; for a general discussion on the slow manifold, see Ford et al. 2000, and references therein), which suggested that gravity waves associated with balanced motions are produced in the course of a flow's evolution, but that these gravity waves are exponentially small in Rossby number. Such an exponential dependence on the Rossby number cannot be caught by standard multi-time-scale asymptotic methods; these typically reveal an algebraic dependence.[3]

Nevertheless, numerical evidence of gravity wave generation from initially balanced flows has been given

---

[2] Contemporaneous work by Molemaker et al. (2005) has revisited these modes in a fluid with a rigid lid, focusing on the growth rates and emphasizing the possibility that these modes may be important in the ocean interior for transferring energy from the balanced manifold to unbalanced motions leading to dissipation at the small scales.

[3] For example, solving (7) perturbatively in $\mathcal{R}$ as in section 3b, will never reveal the exponentially small gravity waves.

←

FIG. 8. Amplitude of the gravity waves, $|\alpha_u|$, as a function of the meridional wavenumber, l, for four values of $\mathcal{R}$: 0.6, 0.4, 0.2, and 0.1. Lines are as in Fig. 7. For finite $\mathcal{R}$, the asymptotic expression underestimates the amplitudes, but it nevertheless captures well the dependence on the meridional wavenumber.
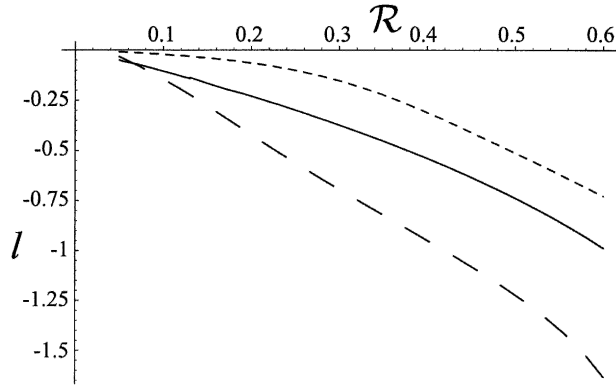
Fig. 10. The value l_0 that maximizes $|\alpha_u|$ in (B8) for each $\mathcal{R}$ (solid line); also plotted are the values of l_{0x} that minimize the difference between the tilts of the balanced edge wave and the gravity wave in the (x, z) plane (long-dashed line), and l_{0y} for the (y, z) plane (short-dashed line).

in the context of frontogenesis (Snyder et al. 1993; Reeder and Griffiths 1996), which emphasized the importance of the time scale of the evolution of the balanced flow, and in the unstable evolution of jets (O'Sullivan and Dunkerton 1995; Zhang 2004).

To our knowledge, theoretical models illustrating a coupling of balanced flow and gravity waves beyond truncated models have been given in only two contexts: in the unstable modes of an axisymmetric vortex and in a horizontal shear.

Ford (1994b) showed that unstable modes of an axisymmetric vortex exist that couple a Rossby wave on the edge of the vortex and gravity waves in the far field. Such modes have also been described as emission of gravity waves from an elliptic vortex, using matched asymptotic expansions (Zeitlin 1991; Ford 1994a; Plougonven and Zeitlin 2002). The gravity waves are excited at the frequency of rotation of the elliptic vortex; hence, this analysis is limited to flows with Rossby number greater than unity (the time scales of the balanced vortex and of the gravity waves are the same, their spatial dimensions differ). Saujani and Shepherd (2002) pointed this out as a weakness, underlining that the small Rossby number regime is the relevant one for geophysical applications.

As an example of a coupling between balanced motions and gravity waves in flows with arbitrary Rossby numbers, Vanneste and Yavneh (2004) have analyzed the excitation of inertia–gravity waves from conditions that are initially balanced, in a horizontal shear, for a stratified fluid. They found that inertia–gravity waves were generated, their amplitude being proportional to $\mathcal{R}^{-1/2} \exp(-K/\mathcal{R})$, where K is a constant.

Our study relates to these previous works in the following ways:

1) The spatial coupling we have studied between a balanced edge wave near the ground and gravity waves aloft is analogous to the one described for unstable modes of an asymptotic vortex (Ford 1994b) between a Rossby wave on the edge of a vortex and gravity waves in the far field. However, whereas the coupling in the case of a vortex is limited to Rossby numbers greater than unity, the coupling in a vertical shear applies for arbitrary Rossby numbers. Finally, whereas radiation is essential to the instability of an axisymmetric vortex, there exist unstable modes in the case of a constant baroclinic shear even with an upper rigid lid (Nakamura 1988; Yamazaki and Peltier 2001b).

2) Interestingly, the dependence in Rossby number of the amplitude of the gravity waves has the same form in Vanneste and Yavneh's (2004) investigation and in ours.[4] However, in contrast to Vanneste and Yavneh, who investigated gravity waves excited from initially balanced conditions (hence a coupling in time), our study focused on the coupling in space.

Note that in the present study and those on the emission of gravity waves from an elliptic vortex, the coupling between gravity waves and balanced motions is not through geostrophic adjustment: balanced motions and gravity waves coexist within each mode. They couple spatially but occupy different regions of space. For the unstable modes, the gravity wave amplitude then grows in time, rather than decaying as in geostrophic adjustment.

8. Summary

We have investigated the spatial coupling of balanced motions and gravity waves in the normal modes of a rotating fluid with linear shear above a rigid lower boundary, using the linearized primitive equations. The key feature of these modes is the spatial transition, at the inertial critical level (IL), from a balanced edge wave near the ground to gravity waves aloft (see Figs. 2 and 3 and the lower panel of Fig. 5). Our interest was to quantify numerically and analytically the amplitude of the gravity waves aloft as a function of the parameters of the problem: the Rossby number $\mathcal{R}$ and the meridional wavenumber l. We have obtained, for neutral solutions with $l = 0$, an exact analytical solution (section 4, Fig. 1). For a given horizontal wavelength, such solutions can only exist if a rigid lid is present at a discrete set of heights, or in an unbounded atmosphere if waves are propagating downward from infinity (section 4).

The more general case of modes with a radiating upper boundary and a nonzero meridional wavenumber l was also considered (section 5, Fig. 5). Such modes appear to be always unstable. The dependence of the

---

[4] It also has the same form as the amplitude of the drag due to topographic gravity waves in the linear study of Muraki (2003, manuscript submitted to *J. Atmos. Sci.*).

gravity wave amplitude for the vertical velocity was shown to have the following behavior for small Rossby number $\mathcal{R}$ [cf. (23)]:

$$|\alpha_u| \sim e^{-\pi l/2} \frac{1}{\sqrt{\mathcal{R}}} \exp\left[-\frac{\pi}{2}\frac{\sqrt{1+l^2}}{\mathcal{R}}\right]. \quad (24)$$

(For clarity, we have set $\bar{\Lambda} = 1$ and $k = 1$.) Hence, these modes provide an illustration of the coupling of balanced motions to gravity waves where the exponential smallness in $\mathcal{R}$ expected from truncated models is confirmed (cf. section 7).

However, as (24) shows, it is not possible to predict the amplitude of the gravity waves from $\mathcal{R}$ alone, and there is an important asymmetry in the dependence on the meridional wavenumber l. For a given Rossby number, we find that there is a meridional wavenumber for which the amplitude of the gravity waves is maximum. As discussed in section 6, we observe that for modes with a radiating upper boundary condition the horizontal wavevector for which the gravity waves are maximal points toward the warm air and is such that the tilts of the balanced edge wave and the gravity waves match smoothly at the IL.

We are presently investigating, in mesoscale numerical simulations with the Weather and Research Forecast Model, the manifestation of these modes and of the role of the IL in more complex flows.

APPENDIX A

Numerical Computations

Two kinds of solutions are displayed in the text: the neutral solution with $l = 0$ (Fig. 1), and radiating, unstable modes without restriction on l (starting from Fig. 5). The technical difficulties in the computation of each kind of solution are different and briefly described below.

a. Neutral solution with l = 0

As explained in the text from the Frobenius analysis, for neutral solutions (σ real) there is only one solution that remains finite at the IL. As noted, calculating this solution by integrating (7) directly from the IL becomes problematic at the CL because of the degeneracy. The

singular point at the CL however is only apparent (Tokioka 1970) and can be removed by an appropriate change of variables, as was shown for meridionally uniform disturbances by Nakamura (1988). We now show that the same is true in general for $l \neq 0$.

Making changes of variables (16) and (17) in (7) yields the following equation for $Y(\xi)$:

$$\xi(1 - \xi^2)Y'' + 2\left(\frac{il}{k}\xi^2 - 1\right)Y' - \xi\overline{\text{Ri}}Y = 0, \quad (A1)$$

where $\overline{\text{Ri}} = \text{Ri}(1 + l^2/k^2) + (1 + il/k)il/k$. Following analogously the calculation of Nakamura (1988), we introduce a function ψ such that

$$Y = \psi - \xi\psi', \quad (A2)$$

such that Eq. (A1) becomes

$$(\xi\partial_\xi - 1)\left[(1 - \xi^2)\psi'' + \frac{2il}{k}\xi\psi' - \overline{\text{Ri}}\psi\right] = 0. \quad (A3)$$

The second-order equation in square brackets no longer indicates a singular point at the CL.

The solution discussed in section 3 was obtained numerically by solving (A3), with $l = 0$ upward and downward from the IL ($\xi = 1$), using standard ODE solvers from the Matlab software. Initial conditions were $\psi(1) = 0$, and an arbitrary value for $\psi'(1)$ with

$$\psi''(1) = -\frac{\overline{\text{Ri}}}{2}\psi'(1). \quad (A4)$$

For $\xi < 0$, the first root of $W(\xi) = 0$ determines the real eigenvalue σ of the mode (and hence the height, in physical space, of the CL).

b. Radiating modes

The solutions for the unstable modes are obtained directly from Eq. (7), that is, in physical coordinate z. This is an eigenvalue problem that obtains both the vertical structure of the modes and their complex phase speed, σ.

Nakamura (1988) and Yamazaki and Peltier (2001b) have carried out similar investigations but with a rigid lid, whereas we will impose a radiating boundary condition. Nakamura used a shooting method, and Yamazaki and Peltier used sparse matrices. We have used both, but will discuss only the shooting method, as an adaptive ODE solver efficiently provides the higher resolution often required near the IL.

Using the explicit Runge–Kutta (4, 5) solver from Matlab, Eq. (7) is solved in the interval $[0, z_{\text{top}}]$, where

$z_{\text{top}} = 20$, typically with a radiating upper boundary condition derived from (15a)

$$w'(z_{\text{top}})(z_{\text{top}} - \sigma) - Pw(z_{\text{top}}) = 0. \qquad \text{(A5)}$$

A Newton method (Tokioka 1970) is used to obtain the eigenvalue σ such that the solution meets the lower boundary condition $w(0) = 0$. The starting point for σ is obtained from the phase speed σ_b expressed in (14) after which continuation is used for varying l. Finally, the solutions are normalized so that $w(z_{\text{CL}}) = 1$.

To assess the validity of the numerically obtained results, it has been checked that results were not sensitive to changes in z_{top}, to the choice and tolerances of the ODE solver, or to the change of (29) to a second-order boundary condition. Results were most sensitive to variations of z_{top}, yet changing z_{top} from 20 to 50 only introduced changes of order 0.001% in σ and 1% in α_u.

The numerical shooting method failed when the imaginary part of σ became too small (of order 10^{-6}) and the sensitivity of the equation to the eigenvalue becomes too large. Hence this method is limited to regions of parameter space for which the growth rates are not too small $[\text{Im}(\sigma) > 10^{-6}]$, that is, corresponding to $\mathcal{R} > 0.3$.

APPENDIX B

Analytical Determination of the Amplitude of the Gravity Waves for the Radiating Modes

As explained in section 4, it is possible to transform (7) into the differential equation for the hypergeometric functions. This allowed an exact analytical determination of the amplitude of the gravity wave part of the solutions for neutral solutions with $l = 0$. For the radiating, unstable modes, we proceed in essentially the same way, but the details differ and a slight approximation is involved.

We consider only modes having complex σ. From the expressions of the indicial roots at the singularities of the equation (AS, section 15.5.2) we know that there are in that case two linearly independent solutions that are well behaved at the IL, $\eta_{\text{IL}} = 1$. Expressions for these two solutions in the neighborhood of the IL are (AS, section 15.5.5–6)

$$Y_1(\eta) = F(a, b, a + b + 1 - c, 1 - \eta) \qquad \text{(B1a)}$$

and

$$Y_2(\eta) = (1 - \eta)^{il/k} F(c - b,$$
$$c - a, c - a - b + 1, 1 - \eta), \qquad \text{(B1b)}$$

where a, b, and c are defined in (19b).

The transformation Eq. (15.3.8) in AS is then used to express Y_1 and Y_2 in terms of hypergeometrics with argument $1/\eta$. Setting these to 1 provides the asymptotic behavior as $|\eta| \to \infty$

$$\text{for} \quad |\eta| \to \infty, \quad Y_1(\eta) \sim A\eta^{-a} + B\eta^{-b} \qquad \text{(B2)}$$

and

$$Y_2(\eta) \sim C\eta^{-a} + D\eta^{-b}. \qquad \text{(B3)}$$

The coefficients A, B, C, and D are functions of the parameters ($\mathcal{R}$, k, l, and $\bar{\Lambda}$).

Working back through changes of variables (16), (17), and (18), we find that the solution having only outgoing waves aloft must have a far-field asymptotic behavior containing only η^{-b}. Hence, solutions of (19) satisfying the outgoing-wave boundary condition are proportional to the combination

$$Y_o(\eta) = CY_1(\eta) - AY_2(\eta). \qquad \text{(B4)}$$

For $|\eta| \to \infty$ the asymptotic form of this solution is $Y_o(\eta) \sim \mathcal{A}\eta^{-b}$, where

$$\mathcal{A} = (-1)^{il/k}|\Gamma(i\mu)|^2|\Gamma(1 + a^* - b)|^2$$
$$\left(\frac{1}{|\Gamma(a^*)|^2|\Gamma(1-a^*)|^2} - \frac{1}{|\Gamma(b)|^2|\Gamma(1 - b)|^2} \right). \qquad \text{(B5)}$$

Next we need to normalize the mode so that $Y(\eta_{\text{CL}}) = 1$, with $\eta_{\text{CL}} = (\mathcal{R}\bar{\Lambda}k)^2(z_{\text{CL}} - \sigma)^2 = -(\mathcal{R}\bar{\Lambda}k)^2(\text{Im}(\sigma))^2$. Now, as we do not know analytically the value of $\text{Im}(\sigma)$, we will make the following approximation: the mode will be normalized so that $Y(0) = 1$. This is the only approximation we make, and as the growth rates of the modes are small, the analytical estimation of the amplitude of the gravity waves will turn out to be remarkably good.

To obtain the values of $Y_1(0)$ and $Y_2(0)$, we now use the transformation (15.3.6) in AS, which yields

$$Y_o(0) = \frac{|\Gamma(1 + a^* - b)|^2 \Gamma(-i\mu)\Gamma\left(\frac{3}{2}\right)}{\Gamma(1 - a)\Gamma(1 - b^*)}$$
$$\left(\frac{(-1)^{il/k}}{\Gamma(a^*)\Gamma(1 - a^*)} - \frac{1}{\Gamma(b)\Gamma(1 - b)} \right). \qquad \text{(B6)}$$

Hence, the normalized solution can be expressed in the far field as

$$\text{for} \quad |\eta| \to \infty, \quad \frac{Y_o(\eta)}{Y_o(0)} \sim \frac{\mathcal{A}}{Y_o(0)} \eta^{-b}. \qquad \text{(B7)}$$

The last step is to work through the changes of variable (16), (17), and (18) to obtain the corresponding expression for α_u:

$$\alpha_u(\mathcal{R}, k, l, \bar{\Lambda}) = (\mathcal{R}\bar{\Lambda}k)^P e^{-\pi l/k} \frac{\Gamma(i\mu)}{\Gamma\left(\dfrac{3}{2}\right)} \Gamma(1-a)\Gamma(1-b^*) \left[\frac{1}{|\Gamma(a^*)|^2 |\Gamma(1-a^*)|^2} - \frac{1}{|\Gamma(b)|^2 |\Gamma(1-b)|^2} \right]$$

$$\left[\frac{e^{-\pi l/k}}{\Gamma(a^*)\Gamma(1-a^*)} - \frac{1}{\Gamma(b)\Gamma(1-b)} \right]^{-1}. \tag{B8}$$

For small Rossby numbers, P is dominated by the term involving $1/\mathcal{R}$. Using properties and asymptotics of the Gamma function (AS, sections 6.1.23 and 6.1.39) results in the asymptotic expression for small $\mathcal{R}$ (23).

REFERENCES

Abramowitz, M., and I. Stegun, Ed., 1964: *Handbook of Mathematical Functions.* National Bureau of Standards, Applied Mathematics Series, Vol. 55, U.S. Government Printing Office, 1046 pp.

Bender, C. M., and S. A. Orszag, 1978: *Advanced Mathematical Methods for Scientists and Engineers.* International Series in Pure and Applied Mathematics, McGraw Hill, 593 pp.

Blumen, W., 1972: Geostrophic adjustment. *Rev. Geophys. Space Phys.,* **10,** 485–528.

Booker, J., and F. Bretherton, 1967: The critical layer for internal gravity waves in a shear flow. *J. Fluid Mech.,* **27,** 513–539.

Braun, M., 1993: *Differential Equations and their Applications.* Springer Verlag, 578 pp.

Charney, J. G., 1947: The dynamics of long waves in a baroclinic westerly current. *J. Meteor.,* **4,** 135–162.

Dewar, W., and P. Killworth, 1995: Do fast gravity waves interact with geostrophic motions? *Deep-Sea Res.,* **42,** 1063–1081.

Eady, E., 1949: Long waves and cyclone waves. *Tellus,* **1,** 33–52.

Ford, R., 1994a: The response of a rotating ellipse of uniform potential vorticity to gravity wave radiation. *Phys. Fluids,* **6,** 3694–3704.

——, 1994b: The instability of an axisymmetric vortex with monotonic potential vorticity in rotating shallow water. *J. Fluid Mech.,* **280,** 303–334.

——, M. E. McIntyre, and W. A. Norton, 2000: Balance and the slow quasimanifold: Some explicit results. *J. Atmos. Sci.,* **57,** 1236–1254.

Gill, A. E., 1982: *Atmosphere–Ocean Dynamics.* Academic Press, 662 pp.

Hoskins, B. J., and F. P. Bretherton, 1972: Atmospheric frontogenesis models: Mathematical formulation and solution. *J. Atmos. Sci.,* **29,** 11–37.

——, M. McIntyre, and A. Robertson, 1985: On the use and significance of isentropic potential vorticity maps. *Quart. J. Roy. Meteor. Soc.,* **111,** 877–946.

Iga, K., 1993: Reconsideration of Orlanski's instability theory of frontal waves. *J. Fluid Mech.,* **255,** 213–236.

Inverarity, G., and G. Shutts, 2000: A general, linearized vertical structure equation for the vertical velocity: Properties, scalings and special cases. *Quart. J. Roy. Meteor. Soc.,* **126,** 2709–2724.

Jones, W., 1967: Propagation of internal gravity waves in fluids with shear flow and rotation. *J. Fluid Mech.,* **30,** 439–448.

Leith, C., 1980: Nonlinear normal mode initialization and quasigeostrophic theory. *J. Atmos. Sci.,* **37,** 958–968.

Lorenz, E., 1980: Attractor sets and quasigeostrophic equilibrium. *J. Atmos. Sci.,* **37,** 1685–1699.

——, and V. Krishnamurty, 1987: On the nonexistence of a slow manifold. *J. Atmos. Sci.,* **44,** 2940–2950.

McIntyre, M., 1965: A separable nongeostrophic baroclinic stability problem. *J. Atmos. Sci.,* **22,** 730–731.

McWilliams, J. C., and P. R. Gent, 1980: Intermediate models of planetary circulations in the atmosphere and ocean. *J. Atmos. Sci.,* **37,** 1657–1678.

Molemaker, M. J., J. C. McWilliams, and P. R. Gent, 2005: Baroclinic instability and loss of balance. *J. Phys. Oceanogr.,* in press.

Nakamura, N., 1988: Scale selection of baroclinic instability—Effects of stratification and nongeostrophy. *J. Atmos. Sci.,* **45,** 3253–3267.

O'Sullivan, D., and T. Dunkerton, 1995: Generation of inertia–gravity waves in a simulated life cycle of baroclinic instability. *J. Atmos. Sci.,* **52,** 3695–3716.

Plougonven, R., and V. Zeitlin, 2002: Internal gravity wave emission from a pancake vortex: An example of wave–vortex interaction in strongly stratified flows. *Phys. Fluids,* **14,** 1259–1268.

Reeder, M. J., and M. Griffiths, 1996: Stratospheric inertia–gravity waves generated in a numerical model of frontogenesis. Part II: Wave sources, generation mechanisms and momentum fluxes. *Quart. J. Roy. Meteor. Soc.,* **122,** 1175–1195.

Sakai, S., 1989: Rossby–Kelvin instability: A new type of ageostrophic instability caused by a resonance between Rossby waves and gravity waves. *J. Fluid Mech.,* **202,** 149–176.

Saujani, S., and T. Shepherd, 2002: Comments on "Balance and the slow manifold: Some explicit results." *J. Atmos. Sci.,* **59,** 2874–2877.

Shen, B.-W., and Y.-L. Lin, 1999: Effects of critical levels on two-dimensional back-sheared flow over an isolated mountain ridge on an *f* plane. *J. Atmos. Sci.,* **56,** 3286–3302.

Shutts, G., 2001: A linear model of back-sheared flow over an isolated hill in the presence of rotation. *J. Atmos. Sci.,* **58,** 3293–3311.

——, 2003: Inertia–gravity wave and neutral Eady wave trains forced by directionally sheared flow over isolated hills. *J. Atmos. Sci.,* **60,** 593–606.

Snyder, C., 1995: Stability of steady fronts with uniform potential vorticity. *J. Atmos. Sci.,* **52,** 724–736.

——, W. Skamarock, and R. Rotunno, 1993: Frontal dynamics near and following frontal collapse. *J. Atmos. Sci.,* **50,** 3194–3211.

Stone, P., 1966: On non-geostrophic baroclinic instability. *J. Atmos. Sci.,* **23,** 390–400.

——, 1970: On non-geostrophic baroclinic instability. Part II. *J. Atmos. Sci.,* **27,** 721–726.

Tokioka, T., 1970: Non-geostrophic and non-hydrostatic stability of a baroclinic fluid. *J. Meteor. Soc. Japan,* **48,** 503–520.

Vanneste, J., and I. Yavneh, 2004: Exponentially small inertia–gravity waves and the breakdown of quasigeostrophic balance. *J. Atmos. Sci.,* **61,** 211–223.

Vautard, R., and B. Legras, 1986: Invariant manifolds, quasigeostrophy, and initialization. *J. Atmos. Sci.,* **43,** 565–584.

Wurtele, M., A. Datta, and R. Sharman, 2000: The propagation of a gravity–inertia wave in a positively sheared flow. *J. Atmos. Sci.,* **57,** 3703–3715.

Yamanaka, M., and H. Tanaka, 1984: Propagation and breakdown of internal inertia–gravity waves near critical levels in the middle atmosphere. *J. Meteor. Soc. Japan,* **62,** 1–17.

Yamazaki, Y. H., and W. R. Peltier, 2001a: The existence of sub-synoptic-scale baroclinic instability and the nonlinear evolution of shallow disturbances. *J. Atmos. Sci.,* **58,** 657–683.

——, and ——, 2001b: Baroclinic instability in an Euler equations-based column model: The coexistence of a deep synoptic-scale mode and shallow subsynoptic-scale modes. *J. Atmos. Sci.,* **58,** 780–792.

Zeitlin, V., 1991: On the backreaction of acoustic radiation for distributed two-dimensional vortex structures. *Phys. Fluids,* **A3,** 1677–1680.

Zhang, F., 2004: Generation of mesoscale gravity waves in upper-tropospheric jet-front systems. *J. Atmos. Sci.,* **61,** 440–457.